Journal of
Marine Science and Engineering

MDPI

Article

Improvement of Propeller Hydrodynamic Prediction Model Based on Multitask ANN and Its Application in Optimization Design

Liang Li [1,2], Yihong Chen [2], Lu Huang [2], Qing Hai [2], Denghai Tang [2] and Chao Wang [1,*]

[1] College of Shipbuilding Engineering, Harbin Engineering University, Harbin 150001, China; heuliliang@foxmail.com

[2] China Ship Scientific Research Center, Wuxi 214082, China; cyh0925@tom.com (Y.C.); huanglu@cssrc.com.cn (L.H.); cssrchq@163.com (Q.H.); dhtang0@163.com (D.T.)

* Correspondence: wangchao0104@hrbeu.edu.cn

Abstract: A multitask learning (MTL) model based on artificial neural networks (ANNs) is proposed in this study to improve the prediction accuracy and physical reliability of marine propeller hydrodynamic performance. The propeller's comprehensive geometric features are used as inputs, and the coefficients of quadratic polynomials for the thrust coefficient (K_T) and torque coefficient ($10K_Q$) curves are predicted as outputs. The loss function is customized through a positive gradient penalty of the curves to accelerate training. When the single-task and multitask models were compared, the prediction errors were reduced; K_T decreased from 2.61% to 2.07%, 10 K_Q decreased from 3.58% to 2.31%, and the efficiency (η) decreased from 3.04% to 2.00%. Non-physical fluctuations in the performance curves were effectively mitigated by the multitask model, yielding predicted curvatures which closely matched the experimental data. Strong generalization was demonstrated when the model was tested on unseen propellers, with deviations of 2.2% for K_T, 4.6% for 10 K_Q, and 3.8% for η. Finally, the model was applied to optimize the propeller design for a 325,000 ton very large ore carrier ship, where a Pareto front with 58 non-dominant solutions for the maximum speed and fluctuating pressure was successfully generated and effectively verified by the model's test results. The model enhanced the prediction of the propeller performance and contributed to optimization in the propeller's design.

Keywords: multitask learning; fast prediction; marine propeller; optimization design; open-water performance

check for updates

Academic Editor: Decheng Wan

Received: 8 January 2025
Revised: 17 January 2025
Accepted: 18 January 2025
Published: 20 January 2025

Citation: Li, L.; Chen, Y.; Huang, L.; Hai, Q.; Tang, D.; Wang, C. Improvement of Propeller Hydrodynamic Prediction Model Based on Multitask ANN and Its Application in Optimization Design. *J. Mar. Sci. Eng.* **2025**, *13*, 183. https://doi.org/10.3390/jmse13010183

1. Introduction

Propellers are the preferred propulsion system for commercial vessels due to their simple design, low manufacturing costs, and reliable propulsion efficiency [1]. As a critical component of the vessel's power system, the propeller plays a significant role in determining the key performance metrics, such as speed and noise levels. Consequently, its design is a crucial aspect of overall ship design [2]. During the propeller design process, hydrodynamic performance must be addressed first, as it is essential for optimizing the matching of the ship-engine-propeller system and directly influences the propeller's load, thrust, and propulsion efficiency. Although methods for predicting a propeller's hydrodynamic performance have been well established, the increasing trend toward larger, faster, and more environmentally sustainable vessels presents new challenges in propeller design [3]. As a result, higher accuracy and faster prediction times for propeller performance are now required. Improving the ability to predict a propeller's hydrodynamic performance has thus become a critical priority for propeller designers.

The hydrodynamic performance of a propeller is primarily represented by its open-water performance curves, which provide a comprehensive description of the propeller's behavior under various operating conditions. Traditional methods for predicting open-water performance include the chart method [4], potential flow method [5], open-water model testing, and computational fluid dynamics (CFD) simulations. However, the chart method is limited to specific propeller series, and the potential flow method often fails to meet design accuracy requirements due to neglecting fluid viscosity. Open-water model testing [6] is regarded as the most reliable and accurate method for predicting propeller performance. However, due to the lengthy test periods and high costs, these experiments are typically reserved for the verification and confirmation of critical design schemes. Over the years, the CFD method has developed to the point where its predictive accuracy can meet the requirements of propeller engineering design. Researchers have established various numerical methods for simulating propeller rotation and predicting open-water performance, including those based on multiple reference frames (MRFs) [7] and the sliding mesh [8] and overset mesh techniques [9]. Furthermore, studies have been conducted on the uncertainty analysis of open-water performance predictions using CFD [10], leading to the development of numerical prediction platforms for propeller hydrodynamic performance, with commercial solvers like Fluent at their core [11]. In response to the increasing demands for improved propeller efficiency, noise reduction, and other performance criteria, global optimization algorithms are being increasingly employed by propeller designers [12,13]. These algorithms facilitate rapid iterative design processes within a larger design space, allowing for the identification of propeller configurations which optimize the overall performance. CFD methods are heavily reliant on computational hardware, and their relatively low computational efficiency remains insufficient to meet the rapid iteration needs of global optimization algorithms. In recent years, machine learning algorithms, particularly artificial neural networks (ANNs), have found widespread application in maritime engineering. These algorithms have demonstrated significant capabilities in nonlinear fitting and rapid prediction across a range of areas, including the design of key ship parameters [14], real-time shaft power estimation [15], and safety evaluations under extreme weather conditions [16]. As a result, machine learning has emerged as a promising tool for advancing the rapid and accurate prediction of a propeller's open-water performance.

Currently, the ANN has established a solid foundation in the prediction of open-water performance for propeller diagrams. In 2002, Feng et al. [17] utilized a neural network with two hidden layers to train the hydrodynamic data of the AU5 series propeller, validating the feasibility of this approach by comparing it with regression analysis data. In 2005 and 2007, Koushan [18,19] developed BP neural network models to calculate the thrust and torque for the Newton-Rader and Gawn-Burrill series of propellers, respectively. In 2006, the U.S. Naval Surface Warfare Center (NSWC) [20] applied ANNs to develop hydrodynamic prediction models for Wageningen B-series and Ka-series ducted propellers. These models were capable of accurately predicting four-quadrant thrust and torque values. In 2010, Zeng et al. [21] employed BP neural networks to train the hydrodynamic performance test data from the semi-submersible propeller series developed by the China Ship Scientific Research Center (CSSRC). The absolute error of the thrust and torque coefficients was within 1%, and this model was subsequently used for rapid multi-objective optimization of ship propellers. In 2015, Marko [22] from the University of Rijeka further refined the neural network prediction model for Ka-series ducted propellers, paving the way for the development of more generalized models for complex hydrodynamic predictions of azimuth thrusters. In

2023, Li et al. [23] constructed a propeller series diagram based on the INSEAN E1619 parent propeller to analyze the applicability of five regression algorithms—RF, AdaBoost, GBDT, SVMs, and ANNs—for digitizing open-water performance data of large skew propellers. The study found that the SVM had the smallest prediction error, reducing the error by more than 20% compared with the traditional linear regression method.

However, the generalization capabilities of the above ANN model are quite limited due to the unique characteristics of the diagrams themselves. These models can only predict performance for the specific diagram configurations they were trained on. In response to this limitation, researchers have been working toward the development of more generalized rapid prediction models for propeller performance. In 2020, Bakhtiari et al. [24] trained a neural network using CFD data and proposed a mathematical function for the open-water hydrodynamic coefficients of low-pitch MCP propellers. In 2022, Qiang et al. [25] collected data from 66 commercial ship propellers and their corresponding open-water test results, using the propeller's main parameters as inputs to build a surrogate model for predicting open-water performance. However, the training dataset was relatively small, and the input parameters were limited to the blade number, area ratio, and pitch ratio at 0.7R. In 2023, Qiang et al. [26] further advanced the use of dimensionality reduction methods for extracting geometric features of propellers. Their findings revealed that automatic feature extraction significantly improved the accuracy of prediction models compared to using full-feature or primary-feature input. In 2024, Li et al. [27] collected a larger and more standard propeller dataset from physical testing. Meanwhile, a dimension reduction method based on comprehensive features was proposed to reduce the data demand for the prediction model training. This helped improve the prediction accuracy effectively and enable the prediction model to identify propeller load variations resulting from overall or local adjustments in pitch distribution.

Despite these advancements in applying machine learning algorithms to propeller design, certain challenges remain. Rapid prediction models for open-water performance still fall short of meeting practical engineering requirements in terms of prediction accuracy, physical reliability, and generalization. For instance, existing models often predict open-water performance at a single advance coefficient without considering the physical correlation between thrust and torque coefficients across different advance coefficients. This omission leads to non-physical fluctuations in the hydrodynamic performance across various conditions for the same propeller, which can introduce errors in the design process.

Therefore, it is essential to integrate physical principles and utilize multitask learning (MTL) methods to develop predictive models for the complete thrust and torque curves of propellers. Compared with single-task learning models, MTL models have the distinct advantage of being able to predict multiple objectives simultaneously within a single framework. In these models, different tasks share model parameters, regularization techniques, and loss functions, allowing them to leverage the correlations between tasks to improve both generalization and predictive performance. Utilizing an ANN for MTL is not a new concept; it was first introduced in the 1990s [28,29], and its effectiveness has been demonstrated in a variety of fields [30,31], including both related and unrelated tasks [32]. The maritime and propulsion fields have also seen applications of this approach. For example, in 2020, Mliglianti et al. [33] developed a data-driven, physics-informed deep neural network using MTL, integrating cavitation tunnel test data and flow characteristics computed by the boundary element method (BEM). This model was designed to predict the cavitation noise spectrum of propellers during the design phase and holds promise for eliminating the need for propeller model testing, thereby accelerating the design process. In 2023, Loukas et al. [34] introduced an MTL-based model for predicting ship fuel consumption which simultaneously forecasts fuel consumption for both the main and auxiliary engines. Validation results showed that this multitask model improved the R^2 scores and reduced prediction errors compared with single-task models. That same year, Liu et al. [35] proposed a multitask deep learning model aimed at analyzing interactions between ships, predicting both ship trajectories and potential collision risks. This model demonstrated a significant improvement in prediction time scales, outperforming other methods by an order of magnitude.

This study addresses the growing demand for improved hydrodynamic performance for marine propellers by developing an experimental dataset for the open-water performance of merchant ship propellers augmented with B-series chart data. Expert knowledge is incorporated, and feature extraction techniques, including the comprehensive feature representation and polynomial fitting methods, are applied to the propeller's geometric parameters and open-water performance curves. Based on this dataset, single-task and MTL models are developed using multilayer ANNs. The effect of varying hidden-layer neuron counts on the prediction accuracy is analyzed, leading to the creation of rapid prediction models for thrust and torque coefficients. A thorough comparison between the multitask and single task models is conducted, focusing on prediction accuracy and the physical realism of the performance curves. The generalization capability of the multitask model is further validated using three previously unseen propellers from the test set. Finally, the multitask prediction model is applied to optimize the propeller of a 325,000 ton VLOC. A multi-objective optimization framework is established by integrating the quantum particle swarm optimization (QPSO) algorithm, targeting both the maximum speed and induced fluctuating pressure performance. Iterative solutions yield an effective Pareto front, and the reliability and rationality of the optimization parameters are thoroughly assessed. The findings provide reliable methods for propeller performance prediction and optimization, offering valuable insights for the application of machine learning algorithms in marine propeller design. The overall research approach is illustrated in Figure 1.

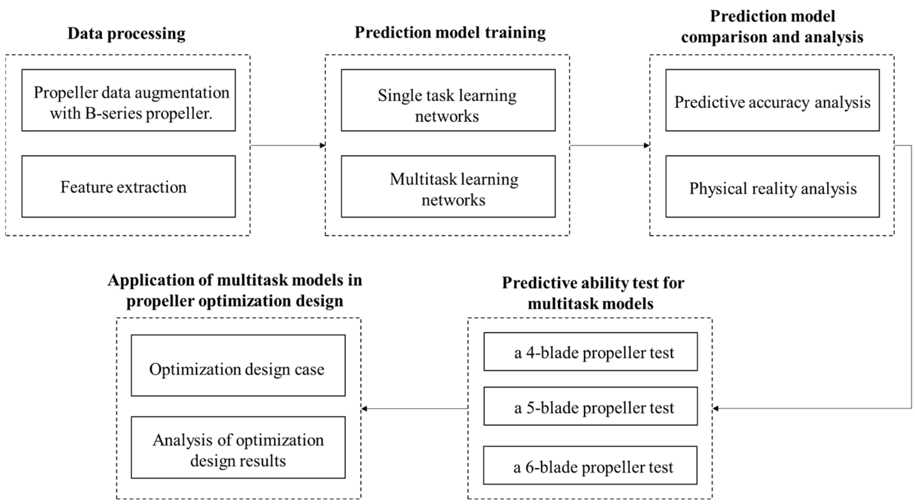

Figure 1. Research design.

2. Data Description

2.1. Data Collection

The dataset used for training the models in this study consisted of two components: proprietary propeller data from the CSSRC and publicly available propeller data from Wageningen B-series diagrams. Figure 2 illustrates the composition of the propeller dataset. The proprietary data from the CSSRC primarily originates from historical open-water propeller tests conducted in a CSSRC towing tank, as well as propeller tests designed by the CSSRC and conducted at other laboratories. These tests encompassed propellers for bulk carriers, container ships, and oil tankers. In total, this dataset includes 127 propellers with complete geometric data and corresponding open-water performance curves. However, the parameter distribution within this dataset is relatively concentrated. As shown in Figure 3, most propellers are four-bladed or five-bladed, with a smaller representation of six-bladed propellers and an almost negligible number of three-bladed propellers. To address this limitation and enhance the dataset, additional data from Wageningen B-series propeller diagrams were incorporated. This augmentation added 126 propeller models with varying blade counts, blade area ratios, and pitch ratios. Figure 4 compares the parameter space distribution of the propeller samples before and after dataset enhancement, focusing on four representative dimensions: blade count, pitch ratio, area ratio, and skew angle. The inclusion of the B-series propeller data significantly expanded the parameter space and yielded a more uniform sample distribution, which would greatly benefit the predictive model's performance by improving its generalization capability. Given the strong similarity in geometric characteristics among the B-series propellers, these data would be used only for training the prediction models to ensure their reliability.

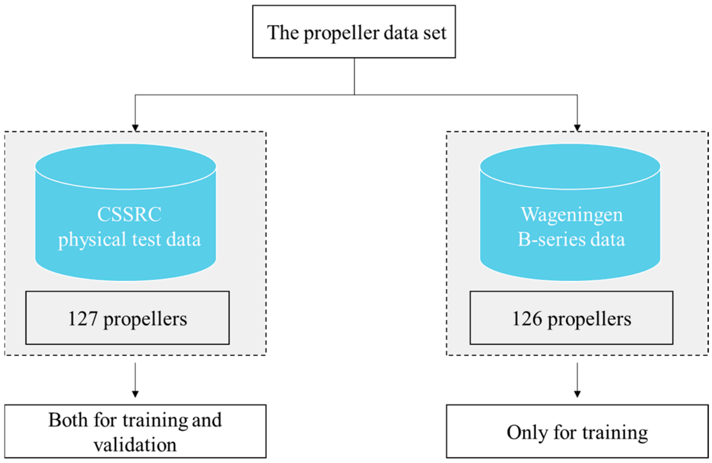

Figure 2. Composition of propeller dataset.

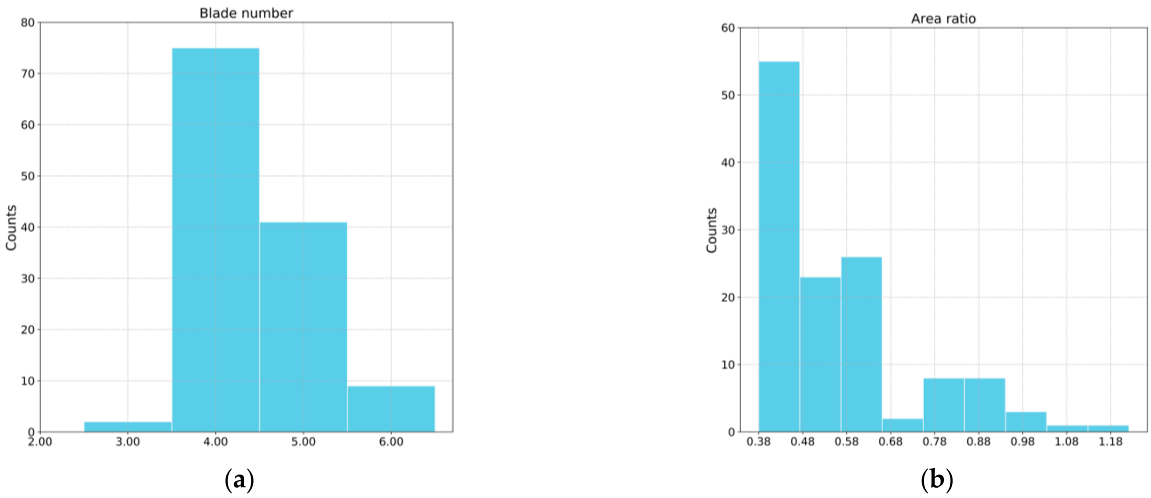

Figure 3. Blade number and area ratio distribution for the CSSRC propeller samples: (**a**) blade number and (**b**) area ratio.

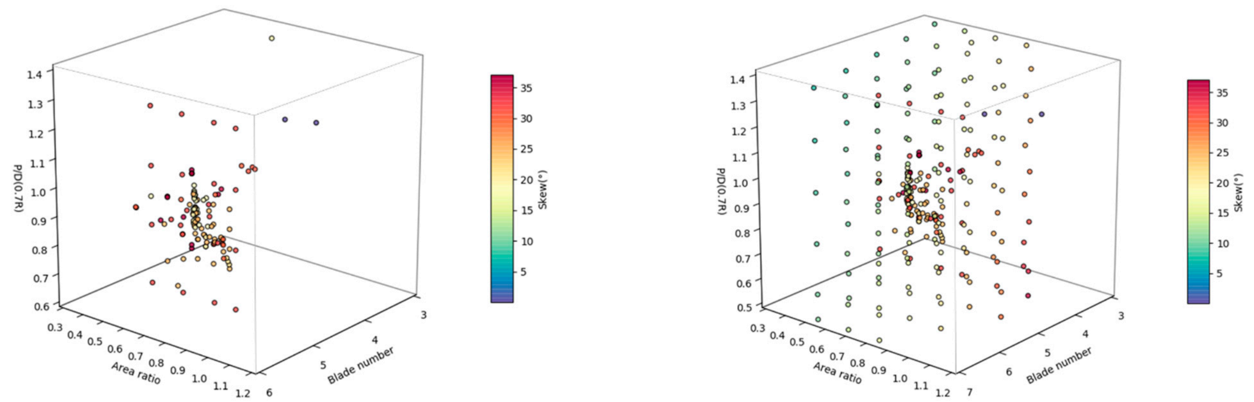

(**a**) (**b**)

Figure 4. Distribution of main parameters for the propeller dataset. (**a**) Only the CSSRC physical test data. (**b**) Data augmentation with B-series propellers.

The raw propeller data included two parts: raw geometric data and raw open-water performance data. Figure 5 presents an example of the standard propeller raw data. In the figure, the geometric data of the propellers include the number of blades, hub ratio, and main parameters. The main parameters consisted of six components: the pitch ratio (P/D), maximum thickness ratio (T_{max}/D), chord length ratio (C/D), skew angle (θ_s), rake ratio (Z_R/D), and maximum camber ratio (f_{max}/C). Here, D is the propeller diameter. The open-water performance data of the propellers included the advance coefficient (J), thrust coefficient (K_T), torque coefficient ($10K_Q$), and open-water efficiency (η). These data were obtained in laboratory conditions by measuring the thrust and torque of the propeller at discrete advance coefficient points. Efficiency was derived from the thrust and torque coefficients, with the specific calculation formulas provided in Equations (1)–(3). Here, n is the rotation speed of the propeller:

$$K_T = \frac{T}{\rho n^2 D^4} \tag{1}$$

$$10K_Q = \frac{10Q}{\rho n^2 D^5} \tag{2}$$

$$\eta = \frac{K_T}{K_Q}\frac{J}{2\pi} \tag{3}$$

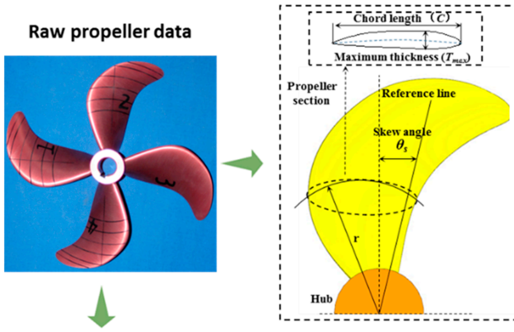

Raw geometric data » Blade number (Z) Hub ratio (H_r)

r/R	P/D	Tmax/D	C/D	θ_s(°)	Zr/D	fmax/C
0.200	1.434	0.032	0.181	0.000	0.000	−0.010
0.300	1.410	0.028	0.200	−2.838	−0.002	−0.021
0.400	1.403	0.024	0.216	−3.243	−0.002	−0.028
0.500	1.371	0.020	0.227	0.000	−0.003	−0.032
0.600	1.302	0.016	0.236	5.676	−0.003	−0.033
0.700	1.177	0.013	0.240	11.757	−0.003	−0.030
0.800	0.974	0.010	0.229	18.108	−0.002	−0.024
0.900	0.719	0.008	0.183	25.946	−0.001	−0.015
0.950	0.578	0.006	0.133	30.270	0.000	−0.008
0.975	0.497	0.004	0.104	32.973	0.001	−0.005
1.000	0.408	0.002	0.076	35.676	0.005	−0.002

Raw open-water performance data

J	0	0.05	0.1	0.15	0.2	0.25	0.3	0.35	0.4	0.45	0.5	0.55	0.6	0.65	0.7	0.75	……
K_T	0.529	0.518	0.505	0.492	0.477	0.462	0.445	0.427	0.408	0.388	0.367	0.345	0.321	0.297	0.271	0.244	……
$10K_Q$	0.693	0.692	0.689	0.683	0.675	0.665	0.653	0.639	0.622	0.604	0.583	0.56	0.534	0.507	0.477	0.445	……
η	0	0.06	0.117	0.172	0.225	0.276	0.325	0.372	0.418	0.46	0.501	0.539	0.574	0.605	0.633	0.654	……

Figure 5. Example of propeller raw data.

2.2. Target Feature Extraction

In previous studies, single-task prediction models were commonly developed using thrust and torque coefficients at individual advance coefficients as target values. However, the lack of correlation between the thrust and torque values at different advance coefficients for the same propeller often leads to characteristic curves with anomalous fluctuations which do not align with the physical reality of the open-water data. To address these issues, this study proposes the development of a multitask prediction model targeting the entire open-water performance curve of a propeller, aiming to improve both modeling efficiency and accuracy. Initially, feature extraction from the propeller's open-water performance data is required. Research indicates that polynomials, as shown in Equations (4) and (5), can achieve high-precision regression for propeller data [36,37]. For a specific propeller, the pitch ratio and area ratio are constants, thus simplifying the formulas for polynomials in terms of the advance coefficient, as shown in Equations (6) and (7). Figure 6 further gives the diagram of feature extraction for a propeller's open-water performance curves using polynomials. This implies that the polynomial coefficients represent all the characteristics of the open-water performance for a given propeller. Differences in open-water performance among various propeller designs can be effectively expressed through these polynomial coefficients:

$$K_T = \sum_{i=1}^{n} C_{Ti} J^{s_i} (\frac{P}{D})^{t_i} (\frac{A_E}{Ao})^{u_i} \tag{4}$$

$$10K_Q = \sum_{i=1}^{n} C_{Qi} J^{s_i} (\frac{P}{D})^{t_i} (\frac{A_E}{Ao})^{u_i} \tag{5}$$

$$K_T = \sum_{i=1}^{n} C_{Ti} J^{s_i} \tag{6}$$

$$10K_Q = \sum_{i=1}^{n} C_{Qi} J^{s_i} \tag{7}$$

J	K_T	$10K_Q$	η
0	0.529	0.693	0
0.05	0.518	0.692	0.06
0.1	0.505	0.689	0.117
0.15	0.492	0.683	0.172
0.2	0.477	0.675	0.225
0.25	0.462	0.665	0.276
0.3	0.445	0.653	0.325
0.35	0.427	0.639	0.372
0.4	0.408	0.622	0.418
0.45	0.388	0.604	0.46
0.5	0.367	0.583	0.501
0.55	0.345	0.56	0.539
0.6	0.321	0.534	0.574
0.65	0.297	0.507	0.605
0.7	0.271	0.477	0.633
0.75	0.244	0.445	0.654
……	……	……	……

Raw open-water performance data

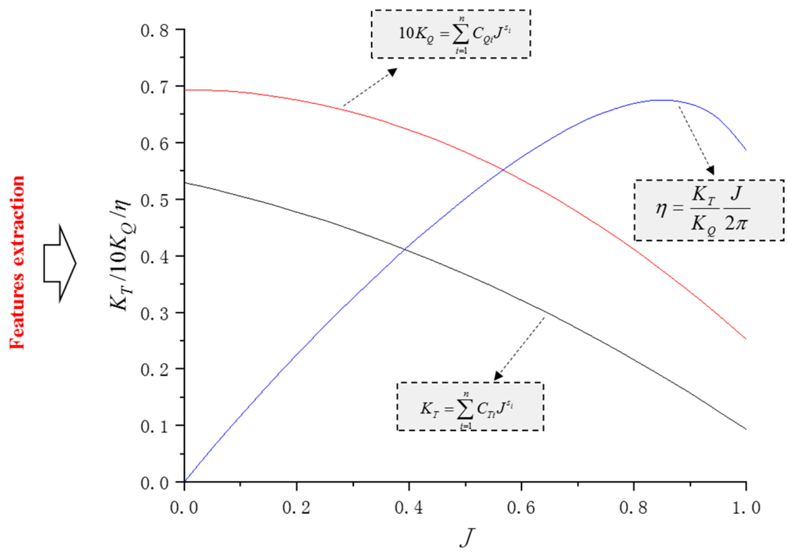

Polynomials expression

Figure 6. Feature extraction for the propeller open-water performance curves using polynomials.

Selecting an appropriate polynomial order is crucial. While higher-degree polynomials can enhance the precision of the representation of propeller open-water characteristic curves, they can also lead to excessive dimensionality of the extracted features, which is detrimental to the construction of open-water performance prediction models. Therefore, both second-order and third-order polynomials, with the advance coefficient as the variable, were used to fit the propeller open-water performance dataset. The following formula was employed to analyze the fitting truncation error:

$$MAPE = \frac{1}{n}\sum_{i=1}^{n}\left|\frac{(\hat{y}_i - y_i)}{y_i}\right| \times 100 \quad (8)$$

where, MAPE is the mean absolute percentage error, $\hat{y}_i$ is the fitted value of the thrust coefficient K_T and torque coefficient K_Q, and y_i is the true value of the thrust coefficient K_T and torque coefficient K_Q. Figure 7 illustrates the truncation errors for the fittings using both second-order and third-order polynomials. For the second-order polynomial, the fitting truncation errors for K_T and $10K_Q$ were approximately 0.4%. In contrast, for the third-order polynomial, the truncation errors for K_T and $10K_Q$ were within 0.2%. This indicates that both second-order and higher-order polynomials can achieve high-precision fitting of the propeller open-water curves. Considering both the dimensionality of the target features and fitting accuracy, a second-order polynomial was selected for feature extraction of the K_T and $10K_Q$ curves of each propeller. Specifically, the feature parameters for the K_T curves were C_{T1}, C_{T2}, and C_{T3}, while those for the $10K_Q$ curves were C_{Q1}, C_{Q2}, and C_{Q3}, as defined by Equations (9) and (10):

$$K_T = C_{T1} + C_{T2}J + C_{T3}J^2 \quad (9)$$

$$10K_Q = C_{Q1} + C_{Q2}J + C_{Q3}J^2 \quad (10)$$

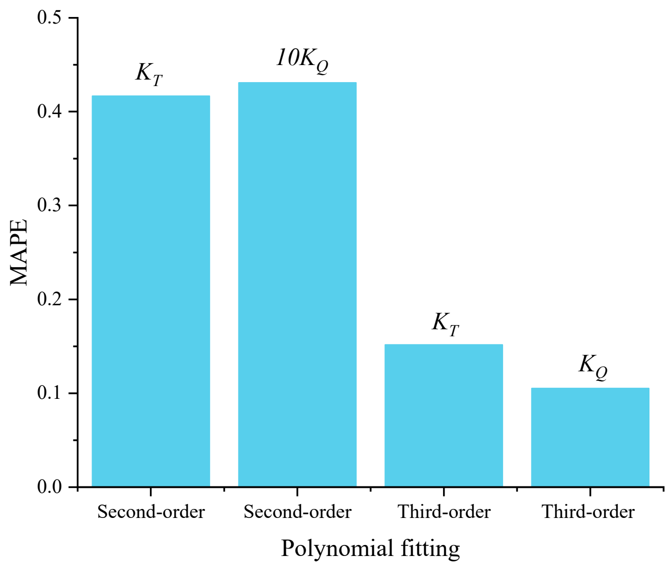

Figure 7. Truncation error for second-order and third-order polynomial fitting.

2.3. Input Feature Extraction

The large number of geometric parameters associated with propellers, which can exceed 100, poses a challenge when all are used as inputs for prediction models. For small sample datasets like those for ship propeller open-water performance, this can lead to the "curse of dimensionality". This not only increases the computational complexity of the model but also significantly reduces the model's generalization ability [38]. To address this issue and enhance the dataset, a statistical representation of the propeller's main parameters was developed, which was proven to be effective in our previous study [27].

This approach has led to the derivation of five comprehensive features, namely the effective pitch, effective camber, area ratio, skew span, and rake span, which describe the radial distribution characteristics of the propeller's pitch, camber, chord length, skew, and rake. The specific derivation process is as follows:

(1) Effective pitch:

$$P_E = \int_{H_r}^{1} rP(r)C(r)dr / \int_{H_r}^{1} rDC(r)dr \tag{11}$$

where r is the radius ratio of the section, H_r is the hub ratio, D is the propeller diameter, $P(r)$ is the pitch ratio distribution in the radial direction, $C(r)$ is the chord length distribution in the radial direction, and P_E is the effective pitch.

(2) Effective camber:

$$\begin{aligned} f_E &= \int_{H_r}^{1} r(f_{\max}(r)/C(r)) \quad C(r)dr / \int_{H_r}^{1} rC(r)dr \\ &= \int_{H_r}^{1} rf_{\max}(r)dr / \int_{H_r}^{1} rC(r)dr \end{aligned} \tag{12}$$

where $f_{\max}(r)$ is the maximum camber distribution of section in the radial direction and f_E is the effective camber.

(3) Area ratio:

$$AEO = A_E / A_o \tag{13}$$

where A_E is the sum of the areas contained in the stretched profile of each propeller blade, which is related to the blade number H_r and $C(r)$, A_o is the disc area ($A_o = \pi R^2$), and R is the propeller radius.

(4) Skew span:

$$\theta_{\text{sa}} = \max(\theta_s(r)) - \min(\theta_s(r)) \tag{14}$$

where θ_{sa} is the skew span, which is calculated by subtracting the minimum skew(min($\theta_s(r)$)) from the maximum skew(max($\theta_s(r)$)) in the radial direction.

(5) Rake span:

$$Z_{Ta} = Z_T(r = 1) - Z_T(r = H_r) \tag{15}$$

$$Z_T(r) = Z_R(r) + r\theta_s(r) \tan \beta_p(r) \tag{16}$$

where Z_{Ta} is the rake span, calculated by subtracting the total rake in the root section ($Z_T(r = 1)$) from the total rake in the tip section ($Z_T(r = 1)$), $Z_R(r)$ is the local rake distribution in the radial direction, and $\beta_p(r)$ is the pitch angle distribution in the radial direction, which can be calculated from the pitch distribution $P(r)$.

The thickness distribution of propeller blades primarily influences the structural design and has a relatively minor impact on hydrodynamic performance. Therefore, it was not considered in this analysis. Ultimately, the input features for the model were selected to include two specific parameters—the number of blades and hub ratio—as well as five comprehensive parameters: the effective pitch, effective camber, area ratio, skew span, and rake span. These parameters collectively served as the input features for the model. Figure 8 presents the process of geometric feature extraction.

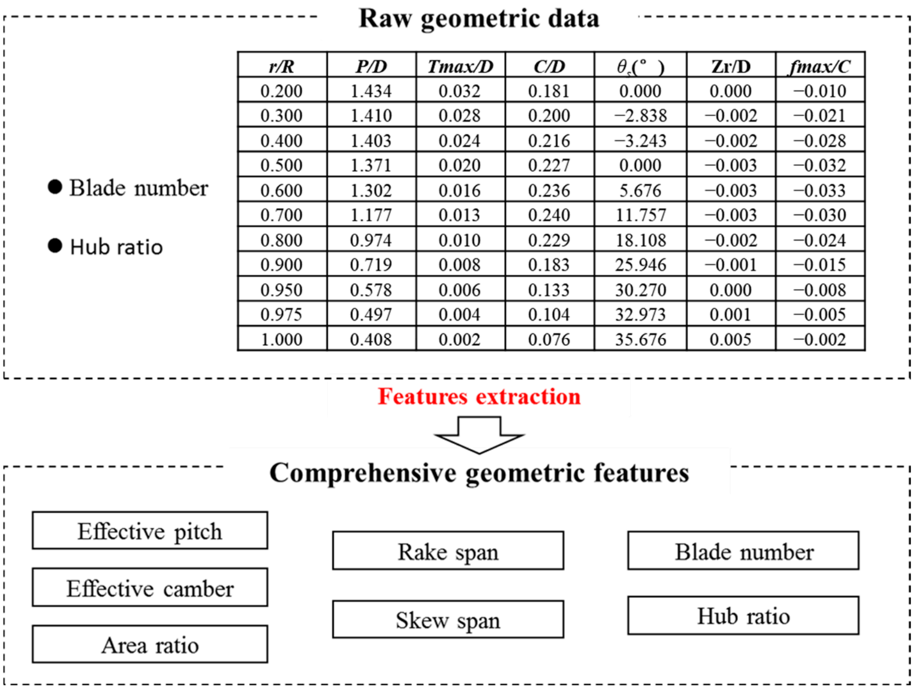

r/R	*P/D*	*Tmax/D*	*C/D*	θ_s(°)	Zr/D	*fmax/C*
0.200	1.434	0.032	0.181	0.000	0.000	−0.010
0.300	1.410	0.028	0.200	−2.838	−0.002	−0.021
0.400	1.403	0.024	0.216	−3.243	−0.002	−0.028
0.500	1.371	0.020	0.227	0.000	−0.003	−0.032
0.600	1.302	0.016	0.236	5.676	−0.003	−0.033
0.700	1.177	0.013	0.240	11.757	−0.003	−0.030
0.800	0.974	0.010	0.229	18.108	−0.002	−0.024
0.900	0.719	0.008	0.183	25.946	−0.001	−0.015
0.950	0.578	0.006	0.133	30.270	0.000	−0.008
0.975	0.497	0.004	0.104	32.973	0.001	−0.005
1.000	0.408	0.002	0.076	35.676	0.005	−0.002

Figure 8. Process of geometric feature extraction.

3. Architecture Design of Artificial Neural Networks

An ANN is a black box model which simulates the functioning of brain neurons and is currently among the leading algorithms in machine learning, with extensive applications in the maritime industry [39,40]. The multi-layer perceptron (MLP) algorithm used in this study is a type of feedforward neural network. It typically comprises one input layer, one output layer, and one or more intermediate hidden layers, with the neurons in each layer fully connected to those in the adjacent layers. The strength of each connection is defined by weights and biases. The input layer is responsible for receiving and transmitting the input data to the hidden layers. Each neuron in the hidden layers computes a weighted sum of its inputs and applies an activation function to pass the result to the next layer. The output layer consists of one or more neurons which receive data from the hidden layers and provide the final output. During the network training process, the weights of the connections are adjusted to minimize the loss function, thereby learning the optimal network parameters suited to the specific dataset. Figure 9 illustrates the operational principle of an artificial neural network.

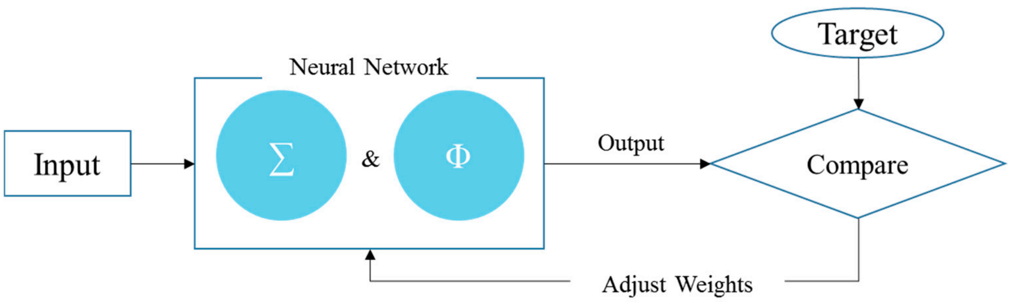

Figure 9. Schematic diagram of neural network, where $\sum$ is a weighted sum and Φ is an activation function.

In this study, the goal of modeling a propeller's open-water performance prediction is to forecast the open-water characteristic curves of a propeller based on specific geometric inputs, framed as a supervised regression learning problem. This problem can be approached using either a single-task learning model or an MTL model. The following sections will introduce both the single-task learning network and the MTL network based on the MLP algorithm.

3.1. Single-Task Learning Networks

In single-task learning modeling, multiple inputs correspond to a single output. This approach is commonly used in existing rapid prediction models for propeller open-water performance. Specifically, the open-water characteristic curves of a propeller are discretized into operational points at specific advance coefficient intervals, with separate models developed to predict the thrust and torque coefficients at each operational point. Figure 10 presents the architecture of the single-task learning network. In this study, separate models were developed for predicting the thrust coefficient and the torque coefficient. While the network architectures and input parameters for both models were identical, the target values differed. The input layer consisted of eight neurons; seven neurons represented the seven geometric feature parameters of the propeller, and one neuron represented the advance coefficient condition. The network included two hidden layers, with the number of neurons in each hidden layer determined based on the specific training requirements of the dataset. Research indicates that an MLP network with two hidden layers can meet the fitting needs of most regression problems. Excessive hidden layers can lead to network complexity, resulting in a significant increase in computational load and a higher risk of overfitting. The output layer contained a single neuron, which corresponded to either the thrust coefficient or the torque coefficient.

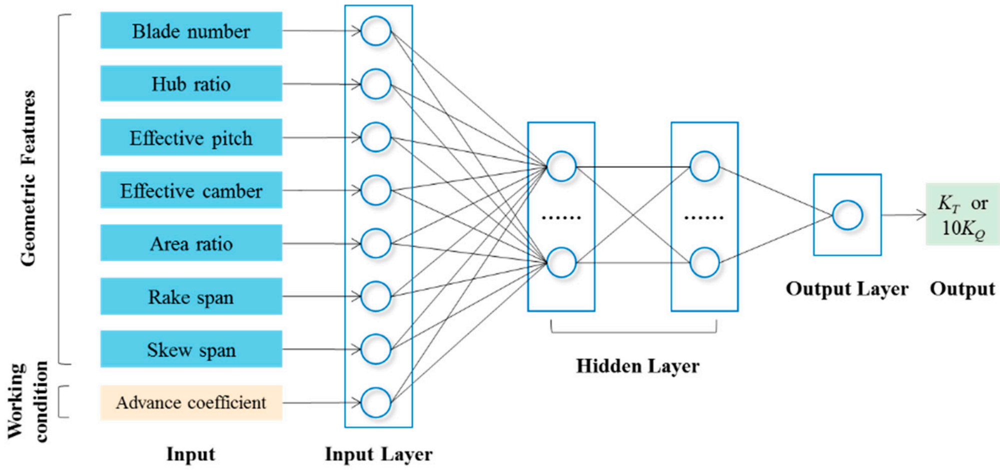

Figure 10. Architecture of single-task learning networks.

The ReLU [41] activation function is employed in the network to implement nonlinear transformations. The function is defined in Equation (17). During backpropagation, the network computes the gradient of the loss function with respect to the weights layer by layer, starting from the output layer. The Adam optimization algorithm [42] is used to optimize the weights and biases until the loss function converges or the number of iterations reaches the preset condition. In single-task learning, the loss function is defined as the mean squared error (MSE), given by Equation (18). Here, $\hat{y}_i$ is the fitted value of the thrust coefficient K_T and torque coefficient K_Q, y_i is the true value of the thrust coefficient K_T and torque coefficient K_Q, and n denotes the number of data points:

$$\mathrm{ReLU}(x) = \max(0, x) \tag{17}$$

$$MSE = \frac{1}{n}\sum_{i=1}^{n}(y_i - \hat{y}_i)^2 \tag{18}$$

3.2. Multitask Learning Networks

In the single-task learning model, the functional form of the propeller's open-water performance curve is not considered. This means that potential functional relationships between the hydrodynamic forces at different operating conditions are ignored. Such relationships not only represent the physical constraints of the propeller's open-water performance but may also contribute to improved modeling accuracy. In contrast, the MTL model does not focus on predicting the hydrodynamic performance at a single advance coefficient. Instead, it directly predicts the polynomial coefficients of the entire open-water thrust coefficient or torque coefficient curves. Figure 11 illustrates the architecture of the MTL network. The number of network layers remained the same as in the single-task learning network, but there were differences in the number of neurons in the input and output layers. Specifically, the number of neurons in the input layer was reduced to seven, focusing solely on the geometric feature parameters. The output layer consisted of three neurons, each corresponding to one of the three quadratic polynomial coefficients for the thrust coefficient curve or the torque coefficient curve.

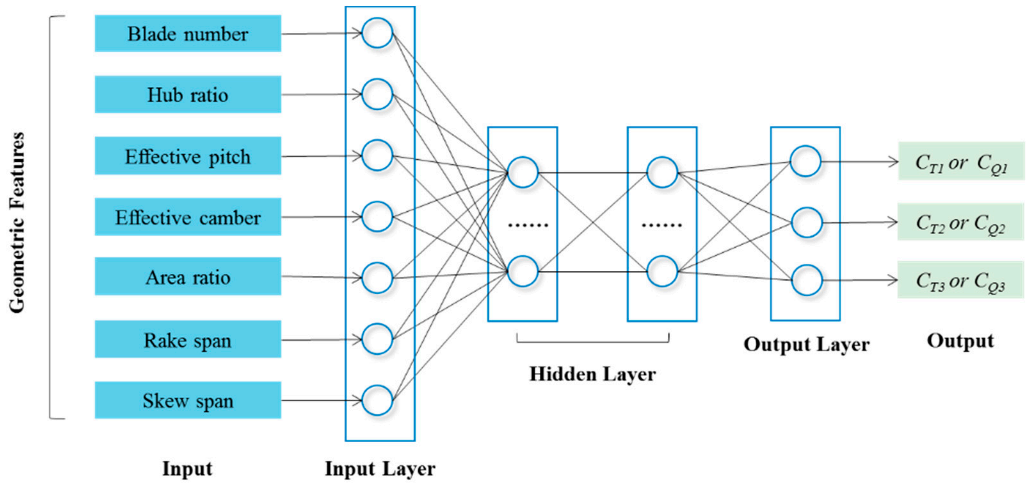

Figure 11. Architecture of multitask learning networks.

In the multitask model, the activation function and iterative optimization algorithm are identical to those used in the single-task learning model. However, a key challenge in MTL is the need to combine the predictions for multiple target variables using methods such as weighted averaging, which guides the model toward optimal performance. For a given target propeller, there can be multiple combinations of quadratic polynomial coefficients which can achieve the desired hydrodynamic curves within a certain forecast error range. Therefore, it is not necessary for all three polynomial coefficients to be strictly the same or extremely close to the target values. This implies that using the MSE of the target values directly as the loss function may not yield the model with the best accuracy.

To address this, a custom loss function is defined for the MTL model. First, the polynomial coefficient predictions and true values are converted into the predicted and actual thrust and torque coefficients within the respective advance coefficient range as described by Equations (9) and (10). Then, the MAPE for each propeller is calculated using Equation (8). The average MAPE error across all samples in the training set is used as the loss function. Additionally, based on physical understanding, in the non-cavitating state and operating within the first quadrant, the thrust and torque coefficients of the propeller decrease as the advance coefficient increases. Therefore, the gradient of the thrust and torque coefficient curves should be negative within the advance coefficient range considered in this study. To incorporate this physical constraint into the model training, a penalty term was added to the loss function to guide the optimization direction [43]. Specifically, if the first derivative of the predicted quadratic polynomial was more than zero, then a significant penalty was applied to the loss function, driving the network model parameters toward optimal values. Figure 12 illustrates the process of customizing the loss function.

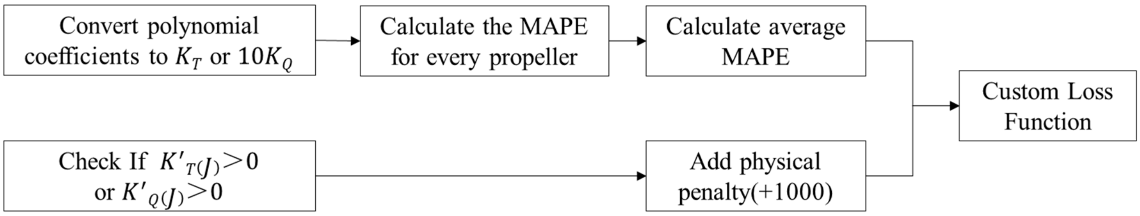

Figure 12. Definition of custom loss function for multitask learning.

4. Modeling Approach

4.1. Model Training Procedure

Figure 13 illustrates the detailed modeling process, with the model training conducted within PyTorch. The dataset was partitioned into three subsets. Initially, three propellers with different numbers of blades (one each with 4 blades, 5 blades, and 6 blades) were randomly selected from the 127 engineering propeller samples to serve as test samples, assessing the model's predictive capability. The remaining 124 engineering propeller samples were then randomly divided into training and validation sets at a ratio of 70% to 30%. Specifically, 87 samples were allocated to the training set, and 37 samples were allocated to the validation set. All 126 B-series propeller samples were included in the training set, resulting in an enhanced total of 213 training samples. Figure 14 presents the propeller dataset partition details in this study.

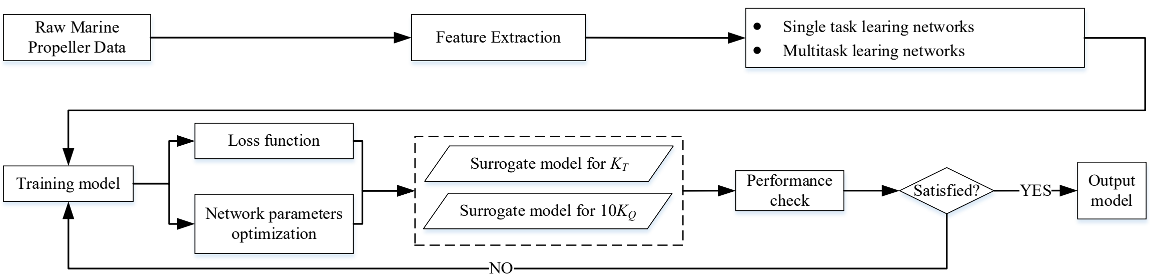

Figure 13. Procedure of the modeling approach.

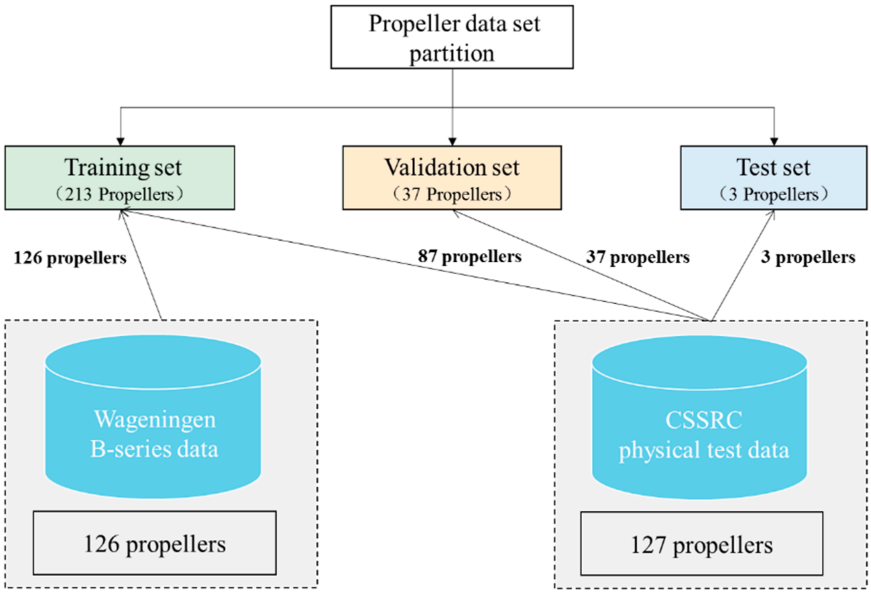

Figure 14. Propeller dataset partition in this study.

It is important to note that the sample size for the MTL model was calculated based on the number of propellers, while for the single-task learning model, it was calculated based on the number of open-water performance data points at different advance coefficients. Thus, for single-task learning, each propeller sample was further divided into multiple samples at various advance coefficients with an interval of ΔJ = 0.05. This aspect is not detailed here. Upon completion of the dataset partitioning, the StandardScaler [44] module was used to standardize the training data. The transformation formula is as follows:

$$X' = \frac{X - \mu}{\sigma} \tag{19}$$

where X' indicates the standardized input variable value, X is the true value of the input variable, μ is the mean of the input variable, and σ is the standard deviation of the input variable.

During the training of neural networks, multiple iterations are required, with each complete iteration referred to as an epoch. In this study, the maximum number of epochs was set to 800. The learning rate is another crucial parameter in training. A learning rate which is too high can cause fluctuations in the optimization process, while a learning rate which is too low can lead to slow convergence. To address this, an adaptive learning rate adjustment strategy was employed using the cosine annealing algorithm [45]. This approach dynamically adjusts the learning rate as described by the following equation:

$$lr = lr_0 \times \cos(\frac{\pi t}{T}) \tag{20}$$

where lr_0 is the initial learning rate (set to 0.005), T is the total number of iterations, and t is the current iteration number. As the number of iterations increases, the learning rate gradually approaches zero. Furthermore, an early stopping mechanism [46] was employed in this study to prevent overfitting. During training, the model's performance on the validation set is continuously monitored in real-time. If the model's performance does not improve for 100 consecutive epochs, it is inferred that the model may have begun to overfit. At this point, the training process is halted prematurely, and the model with the best performance recorded prior to the early stopping trigger is returned.

4.2. Neuron Number Selection

The number of neurons in the hidden layers of a neural network significantly impacts the model's prediction accuracy. Currently, there are no definitive rules for determining the optimal number of hidden layer neurons; it often requires empirical testing based on the specific learning problem. For example, Dalheim et al. [47] investigated the impact of varying hidden layer neuron counts on shaft power prediction. In this study, various neuron counts ranging from 8 to 100 were tested through network training. The optimal number of hidden layer neurons was determined by comparing the prediction errors of the validation set.

Figure 15 illustrates the distribution of validation set errors for various numbers of hidden layer neurons in an MTL network. The heatmap reveals that the overall error for the torque coefficient prediction model was higher compared with the thrust coefficient prediction model. Additionally, as the number of hidden layer neurons increased, the prediction errors for both models decreased, with most high-error values concentrated in the range of fewer than 20 neurons. Table 1 presents the optimization results for the number of hidden layer neurons. For the single-task learning networks, the optimal numbers of hidden layer neurons were 56 and 20 for the thrust coefficient prediction model and 52 and 88 for the torque coefficient prediction model. For the MTL networks, the optimal numbers of hidden layer neurons were 48 and 100 for the thrust coefficient prediction model and 92 and 16 for the torque coefficient prediction model.

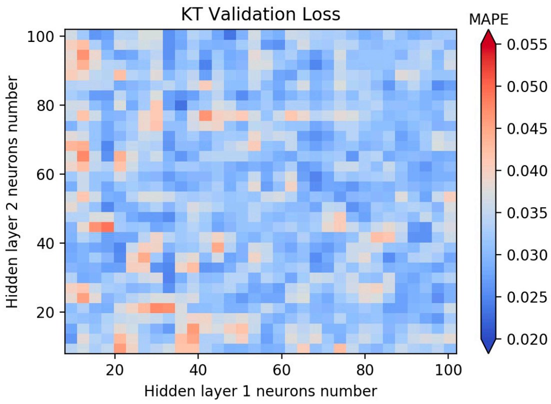

(a)

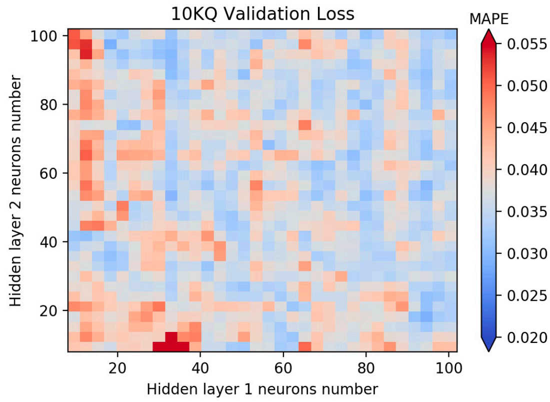

(b)

Figure 15. Validation loss map of multitask learning networks for different numbers of hidden neurons: (**a**) K_T validation loss and (**b**) $10K_Q$ validation loss.

Table 1. Best neuron numbers for the hidden layers.

Hidden Layer	Single-Task Learning Networks		Multitask Learning Networks	
	K_T	$10K_Q$	K_T	$10K_Q$
Hidden layer 1	56	52	48	92
Hidden layer 2	20	88	100	16

5. Comparison of Single-Task and Multitask Models

5.1. Predictive Accuracy

The prediction accuracy of the two models was evaluated as follows. For both models, each propeller's hydrodynamic prediction curve was discretized at intervals of $\Delta J = 0.05$, and the MAPE between the predicted and actual experimental values over the entire advance coefficient range was calculated. This was further used to compute the MAPE for all test cases in the validation set. Table 2 presents the prediction accuracy for the single-task and MTL models on the validation set.

Table 2. Prediction error of ANN model in validation set.

Network Type	Baseline for the MAPE Calculation	Average MAPE (%)		
		K_T	$10K_Q$	η
Single-task model	Model test value	2.61	3.58	3.04
Multitask model	Second-order polynomial fitting value	2.01	2.32	2.20
	Model test value	2.07	2.31	2.38

For the single-task model, the average prediction errors compared with the model test data were as follows: 2.61 for K_T, 3.58 for $10K_Q$, and 3.04 for η. For the multitask model, MAPE calculations were compared against two benchmarks: the second-order polynomial fit results of the model test data and the original model test data. The analysis showed minimal differences between these benchmarks. The average prediction errors were 2.01 and 2.07 for K_T, 2.32 and 2.31 for $10K_Q$, and 2.20 and 2.38 for η, respectively. This indicates that although the second-order polynomial fitting of the hydrodynamic performance curves introduced a truncation error of approximately 0.4%, this error did not accumulate significantly in the model prediction errors, thereby validating the effectiveness of the feature extraction for hydrodynamic performance. When comparing the prediction accuracy while using the original model test data as a benchmark, it is evident that the multitask model achieved a notable improvement over the single-task model. Specifically, the average prediction error for K_T decreased from 2.61 to 2.07, reflecting a relative improvement of approximately 21%. For $10K_Q$, the average prediction error decreased from 3.58 to 2.31, showing a relative improvement of about 35%. Finally, for η, the average prediction error decreased from 3.04 to 2.0, indicating a relative improvement of about 35%.

Figure 16 further illustrates the distribution of prediction errors on the validation set for both models. Errors exceeding 5% were considered large. For the single-task model, there were two instances of large prediction errors for the thrust coefficient K_T, five instances for the torque coefficient $10K_Q$, and four instances for the efficiency η. In contrast, for the multitask model, both the number and value of the large prediction errors decreased. Specifically, the maximum MAPE decreased from 7.43 to 6.19 for the thrust coefficient, from 10.21 to 7.19 for the torque coefficient, and from 7.25 to 6.97 for the efficiency. This indicates that the MTL model performed better than the single-task model in reducing large prediction errors. Increasing the number of propeller samples and improving the completeness of the geometric input features were expected to further enhance the accuracy of the prediction model and reduce extreme errors.

Figures 17 and 18 show the true value against the predicted value given by the multitask model for K_T and $10K_Q$ in the validation data. In these plots, the red solid line represents the best linear regression fit between the predicted and actual values, while the black dashed line represents the 45° perfect fit line. The square scatter points indicate the discrete hydrodynamic results for each propeller in the validation set at various advance coefficients. For the single-task model, the correlation coefficients R for K_T and $10K_Q$ were 0.9976 and 0.9967. For the multitask model, the correlation coefficients for K_T and $10K_Q$ were 0.9981 and 0.9975. The slightly higher R values in the multitask model indicate a stronger correlation between the predicted and actual values, confirming that the multitask model captured the true relationships more effectively. It is also worth noting that the improvement in prediction accuracy using the multitask model was mainly observed in the mid-range of the thrust and torque coefficient values. This region corresponds to the typical operating conditions of propellers in design scenarios, representing common load points.

Enhancing the prediction accuracy in this area is particularly beneficial for improving the overall "ship-engine-propeller" matching performance.

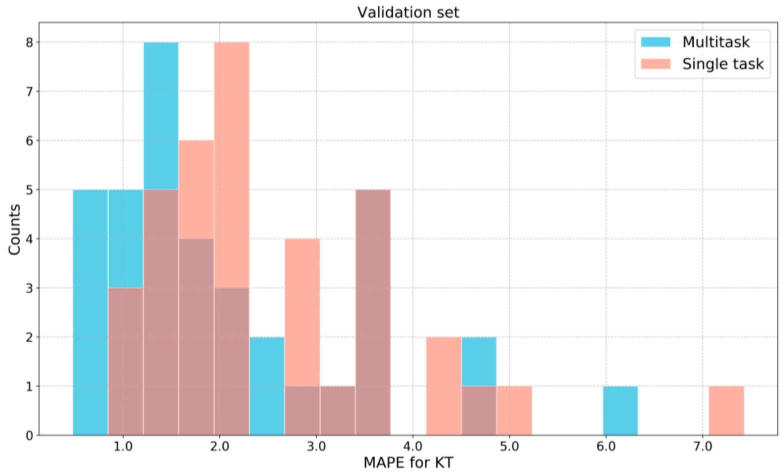

(**a**)

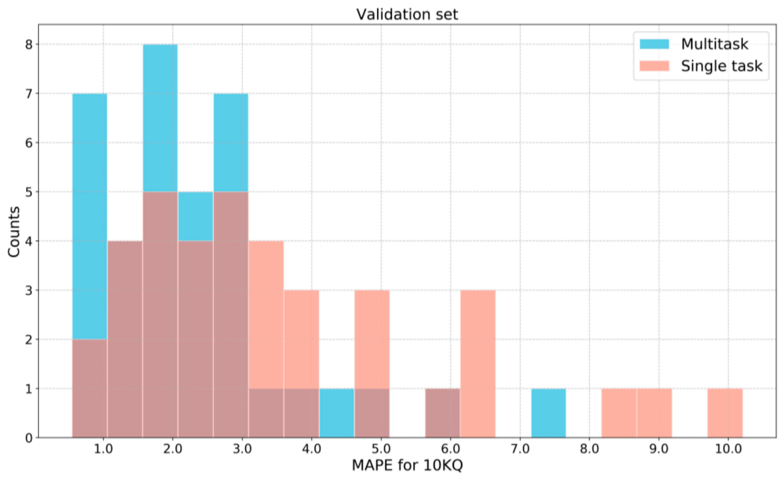

(**b**)

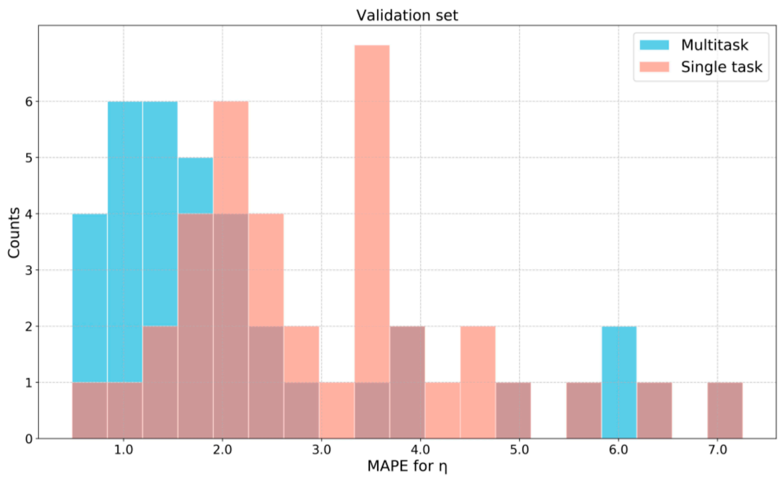

(**c**)

Figure 16. Prediction error histogram of ANN model in validation set: (**a**) K_T; (**b**) $10K_Q$; and (**c**) η.

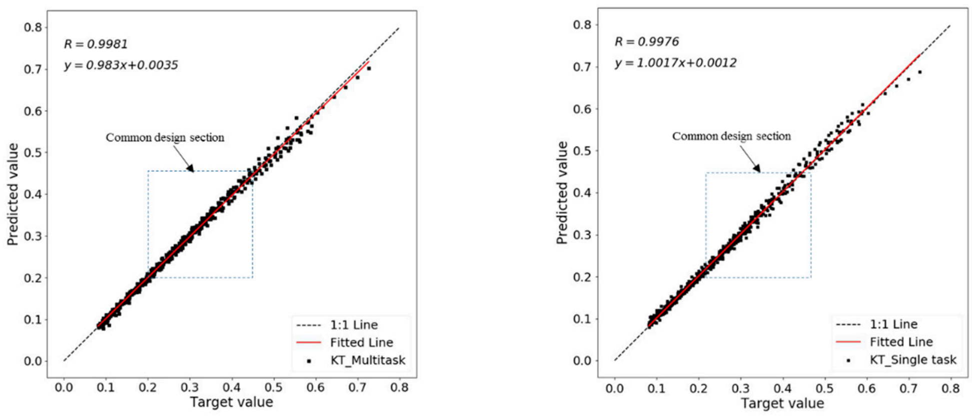

(**a**) (**b**)

Figure 17. True propeller thrust coefficient against predicted value of ANN model in validation set: (**a**) multitask model and (**b**) single-task model.

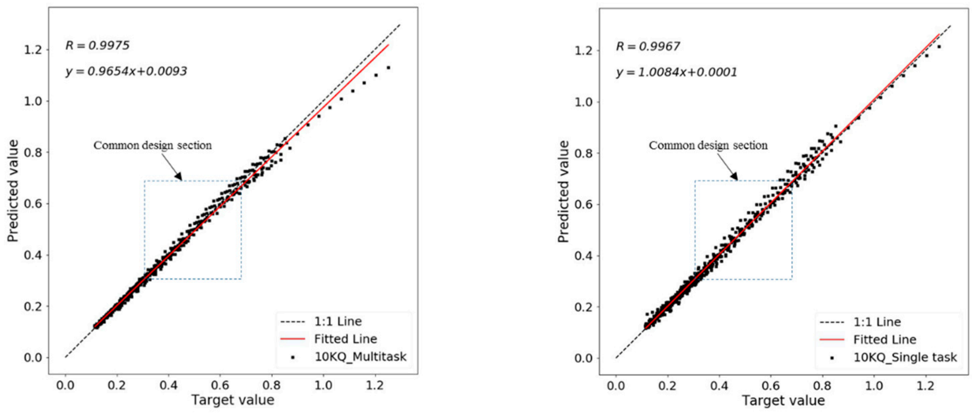

(**a**) (**b**)

Figure 18. True propeller torque coefficient against predicted value of ANN model in validation set: (**a**) multitask model and (**b**) single-task model.

5.2. Physical Reality of Performance Curve

One major issue with the single-task learning model is that it overlooks the correlation and continuity of hydrodynamic coefficients between different advance coefficients for a propeller. This often results in physically unrealistic oscillations in the open-water performance curves. If such oscillations occur near the design point, then they can easily mislead propeller designers, causing inaccuracies in predicting hydrodynamic loads and ship speed. In Figure 19, a typical propeller from the validation set is used to illustrate the comparison of hydrodynamic curves predicted by different models. For the torque coefficient curve, the single-task model showed significant concave oscillations in the Zone1 and Zone2 regions. Correspondingly, the efficiency curve displayed abnormal convex behavior. In contrast, the multitask model, which predicted the entire hydrodynamic curve, significantly improved the smoothness and consistency of the predicted curve.

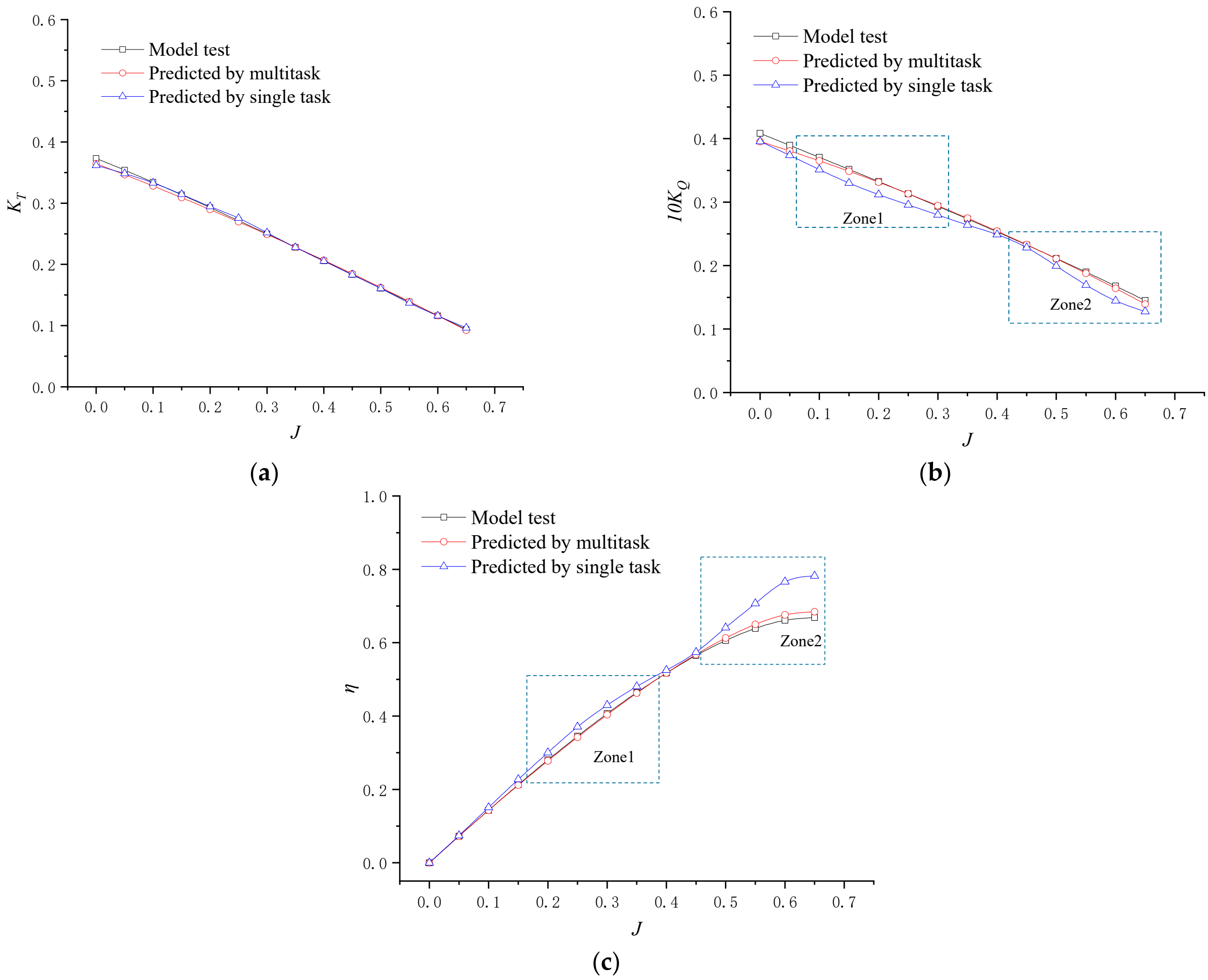

Figure 19. Comparison of propeller efficiency curves for a typical propeller in the validation set: (**a**) K_T; (**b**) $10K_Q$; and (**c**) η.

The smoothness and oscillations of a curve can be represented by its curvature. The formula for calculating the curvature k is provided in Equation (21), where y' is the first derivative and y'' is the second derivative of the curve. Figure 20 presents a comparison of the average curvature across different points on the thrust coefficient and torque coefficient curves predicted by the two models. The efficiency curve is excluded from this discussion due to the significant curvature variations near the point of maximum efficiency, which would dominate the overall curvature analysis:

$$k = \frac{|y''|}{(1 + y'^2)^{1.5}} \tag{21}$$

The results show that the curvature patterns for the predicted thrust and torque coefficient curves were consistent between both models. However, the multitask model predicted curvature values which were closely aligned with the experimental results, whereas the single-task model predicted significantly higher curvature values. This indicates that the hydrodynamic curves predicted by the multitask model exhibited better smoothness, more closely approximating the actual physical behavior. At the same time, because the hydrodynamic curves in the multitask model were represented by quadratic polynomials, the resulting predictions may have been overly smooth. This would lead to slightly lower curvature values compared with the experimental data, smoothing out some of the real fluctuations present in certain propeller designs.

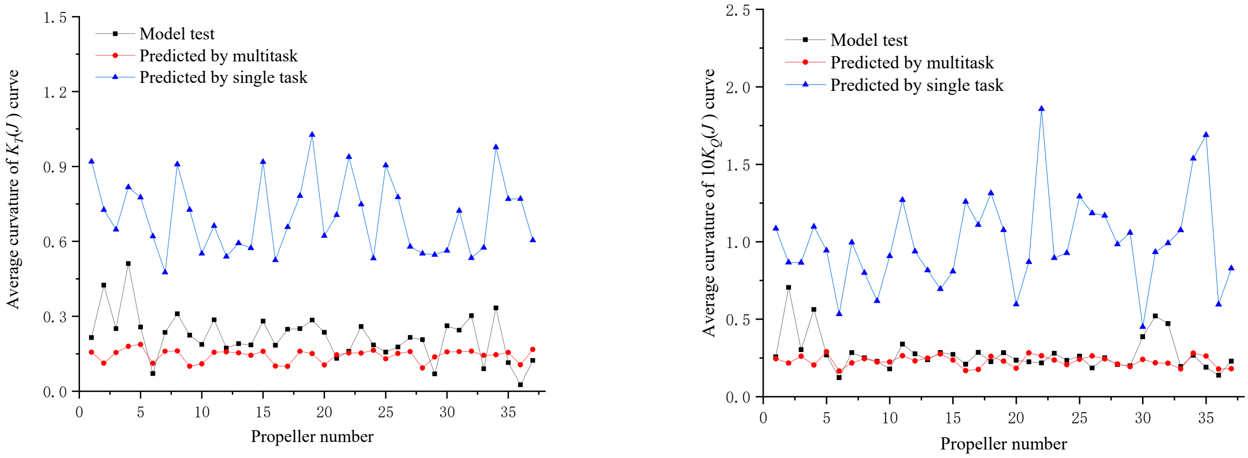

(**a**) (**b**)

Figure 20. Comparison of average curvature of propeller hydrodynamic coefficients curves in validation set: (**a**) K_T and (**b**) $10K_Q$.

6. Application of Multitask Models in Propeller Optimization Design

6.1. Predictive Ability Test for Multitask Models Using Unseen Propellers

Before applying the multitask model to propeller optimization design, its predictive capability for open-water performance was further validated using propellers outside of the training dataset. Three previously unseen propellers with varying blade counts were selected for this purpose. Table 3 presents the geometric parameters and 3D models of the test cases. The test cases included a four-blade propeller (No. 1), a five-blade propeller (No. 2), and a six-blade propeller (No. 3).

Table 3. Geometry parameters for the three propellers in the test set.

Geometry Parameter	Propeller Model		
	No. 1	No. 2	No. 3
Blade number	4	5	6
Hub ratio	0.15	0.15	0.18
Effective pitch	0.8238	0.8375	1.0279
Effective camber	0.02	0.0205	0.0164
Area ratio	0.4023	0.5516	0.8023
Skew span (°)	18.61	32.05	36.71
Rake span	0.0236	0.051	0.0763
Geometry model	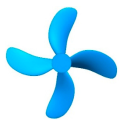	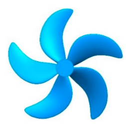	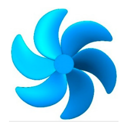

Figure 21 presents the comparison between the multitask model predictions and experimental results for each case, where the scatter points represent the experimental data and the curves represent the predicted values. Table 4 further summarizes the prediction error statistics. Overall, the multitask model's predictions aligned well with the experimental results. The prediction error for the thrust coefficient was within 2.2%, the torque coefficient error was within 4.6%, and the efficiency deviation was within 3.8%, demonstrating the model's generalization capability. Among the three test cases, the largest prediction error was observed for the six-blade propeller (No. 3), which may be attributed to the relatively smaller proportion of six-blade propellers in the training dataset. Table 5 provides a statistical summary of the parameter distribution within the dataset used in this study and outlines the recommended parameter ranges for the multitask prediction model.

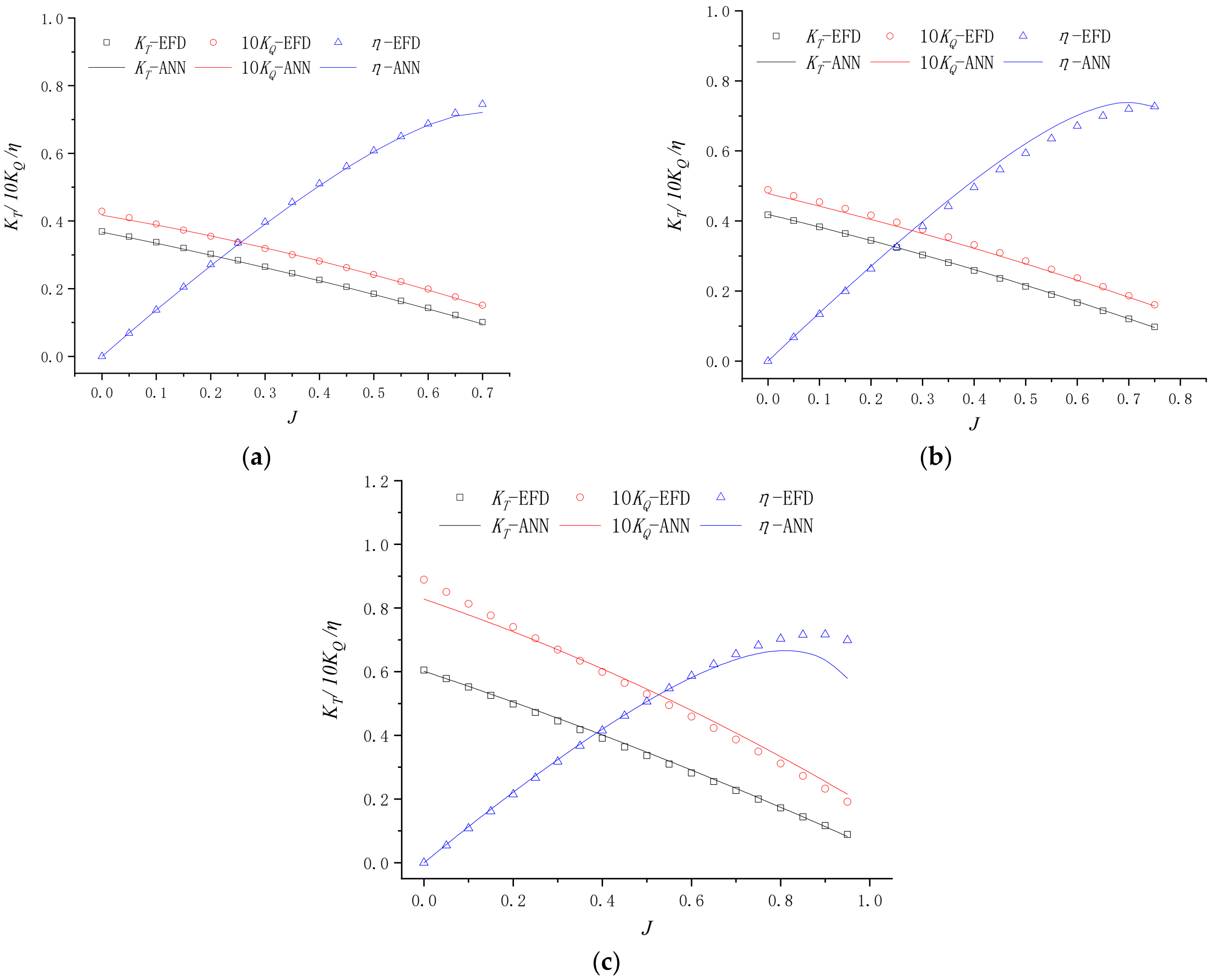

Figure 21. Predictive results of the multitask model for the propeller in the test set: (**a**) No. 1; (**b**) No. 2; and (**c**) No. 3.

Table 4. Prediction accuracy of multitask learning model for the test set.

Propeller Model	MAPE (%)		
	K_T	$10K_Q$	η
No. 1	1.48	0.97	1.05
No. 2	0.82	2.69	3.14
No. 3	2.13	4.56	3.80

Table 5. Recommended parameter ranges for the multitask ANN models to predict the open-water performance.

Range	Blade Number	Hub Ratio	Effective Pitch	Effective Camber	Area Ratio	Skew Span	Rake Span
Minimum	4	0.13	0.50	0.015	0.35	16°	0
Maximum	6	0.21	1.40	0.030	1.22	36°	0.19

6.2. Propeller Optimization Design Application Case

The multitask neural network prediction surrogate model demonstrated both high precision and exceptional efficiency. The prediction time for the open-water performance of a single propeller was reduced to under one second. This capability effectively addresses the challenge of high time costs associated with rapid iterative predictions for a large number of design scenarios. In this study, the optimization of a propeller for a 325,000 ton very large ore carrier (VLOC) was undertaken as a case study. The key geometric parameters of the propeller are presented in Table 6, while the known design inputs are detailed in Tables 7 and 8. This propeller design has a real-world engineering application background and is supported by a complete set of model test data, making it an ideal case for validating the effectiveness of the proposed methodology. Figure 22 illustrates the models and test images of the ship hull and propeller.

Table 6. Main parameters of original propeller for 325,000 ton VLOC.

Parameter	Diameter (m)	Blade Number	Area Ratio	Pitch Ratio (0.7R)	Effective Pitch	Skew Span (°)
Value	10.8	4	0.386	0.7955	0.7894	24.91

Table 7. Propeller design inputs for 325,000 ton VLOC.

Input Parameter	Delivered Power	Host Speed	Thrust Deduction	Wake Fraction	Relative Rotation Efficiency
Value	15,366 kW	55.8 r/min	0.198	0.262	1.004

Table 8. Effective power curve data for 325,000 ton VLOC.

Speed (kn)	8	9	10	11	12	13	14	15	16
Effective power (kW)	1745.5	2494.6	3430.4	4573.3	5946.3	7576.1	9494	11,737.2	14,349.7

(**a**) (**b**)

Figure 22. Model photos of 325,000 ton VLOC and its original propeller: (**a**) hull model; (**b**) propeller model.

The optimization algorithm utilized in this study was the quantum particle swarm optimization (QPSO) method. Two performance metrics were selected as evaluation criteria: the maximum ship speed and propeller-induced fluctuating pressure. The prediction of open-water performance was carried out using the multitask neural network surrogate model developed earlier, while the fluctuating pressure induced by the propeller was estimated using the nonlinear regression rapid prediction model developed by the CSSRC [48]. Four primary design parameters—the propeller diameter, pitch ratio, area ratio, and skew span—were chosen for optimization. The ultimate objective was to maximize the ship speed while minimizing the propeller-induced fluctuating pressure. Additionally, to ensure compatibility between the ship, engine, and propeller, the variation in the design's matching rotational speed with the main engine was restricted to within 5%. Any optimization schemes failing to meet this constraint were penalized using a penalty function. Based on the recommended parameter ranges for the predictive model, as outlined in Table 5, the upper and lower bounds for the optimization parameters were set as shown in Table 9. The multi-objective propeller performance optimization framework established in this study is illustrated in Figure 23. In the figure, N_s is the predicted propeller rotation speed, and N_0 is the host speed.

Table 9. Optimization ranges of the main parameters for the 325,000 ton VLOC propeller.

Range	Diameters	Effective Pitch	Area Ratio	Skew Span
Minimum	9.5	0.6	0.3	15°
Maximum	12	1.0	0.5	30°

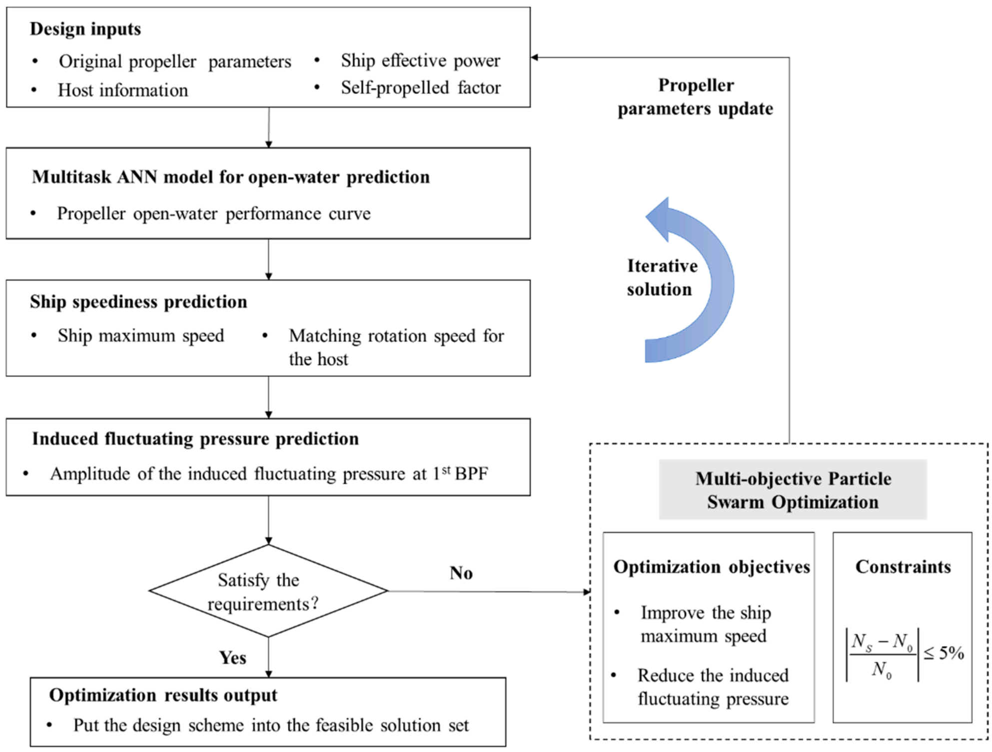

Figure 23. Multi-objective optimization design process for the 325,000 ton VLOC propeller.

6.3. Analysis of Optimization Design Results

The optimization process was conducted using a particle population of 200, a maximum iteration count of 80, and an innovation parameter α = 0.8. Here, α is primarily used to adjust the optimization capability of the algorithm. When α is larger, the algorithm exhibits a stronger global optimization ability, while a smaller α enhances the local optimization capability. The resulting Pareto front solution set, shown in Figure 24, consisted of 58 non-dominated optimal solutions. A trade-off relationship was observed; as the maximum ship speed increased, the fluctuating pressure also rose. Certain regions of the solution set appeared sparse, primarily due to penalty constraints imposed by the mismatch in rotational speed.

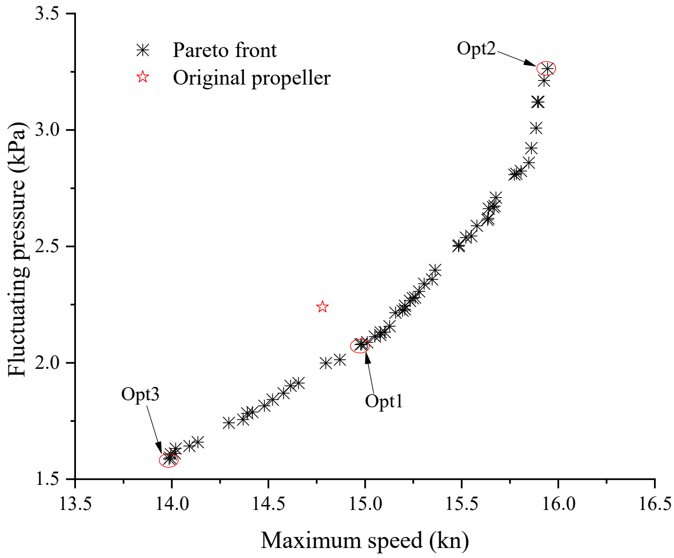

Figure 24. Pareto front for maximum speed and fluctuating pressure.

In Figure 24, the pentagram symbol represents the performance prediction results of the original design. A comparison between the predicted results of the original design and the experimental data is provided in Table 10, with experimental photos shown in Figure 25. Overall, the predictions closely matched the experimental data, with the maximum speed prediction error being 1.65%, the matching rotational speed error being 2.11%, and the first-order blade frequency amplitude error of the induced fluctuating pressure being 4.19%. These findings indirectly validate the reliability of the optimization results.

Table 10. Prediction result validation for the original propeller.

Performance	Prediction Method		Error (%)
	Model Test	Surrogate Model	
Maximum speed (kn)	14.54	14.78	1.65
Rotation speed (r/min)	56.30	57.49	2.11
Fluctuating pressure at 1BPF (kPa)	2.15	2.24	4.19

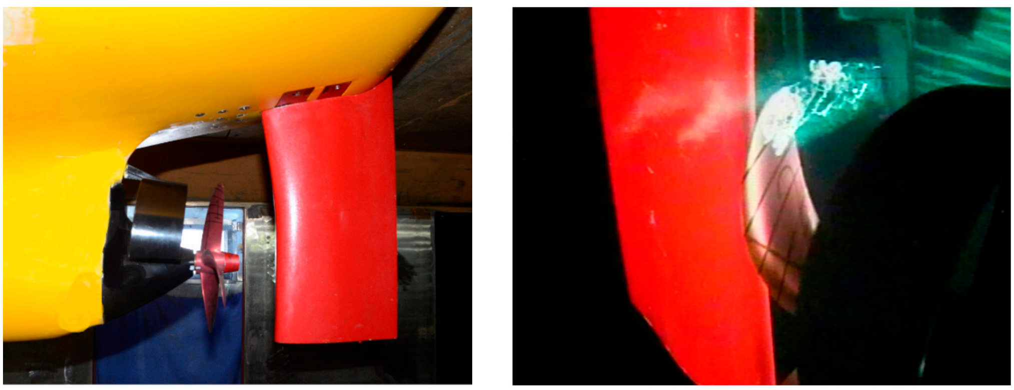

(**a**) (**b**)

Figure 25. Experimental photos of the original propeller: (**a**) the installation photo; (**b**) the cavitation photo.

Three optimized solutions from the Pareto front were selected for further analysis: Opt1, Opt2, and Opt3. Opt1 represented a mid-range solution in the Pareto front, demonstrating moderate improvements in both the maximum ship speed and fluctuating pressure compared with the original design. Opt2, located at the upper edge of the Pareto front, achieved the highest ship speed but also exhibited the highest fluctuating pressure, resulting in inferior vibration and noise characteristics. Opt3, located at the lower edge of the Pareto front, had the lowest fluctuating pressure. However, this came at the cost of a reduced ship speed, resulting in lower propulsion efficiency and economic viability.

Table 11 provides a detailed comparison of the design parameters and performance metrics for the three optimized propeller solutions and the original design. Opt2 achieved improved propulsion efficiency and a higher maximum speed by increasing the diameter and reducing the area ratio. However, the increased diameter reduced the clearance between the blade tip and the ship's stern, resulting in a significant rise in induced pressure fluctuations. Conversely, Opt3 minimized pressure fluctuations by reducing the diameter and increasing the area ratio, but this came at the cost of a lower maximum speed and reduced propulsion efficiency. Opt1 represented a balanced solution. By moderately increasing the propeller diameter, it enhanced the speed performance, while adjustments to the area ratio and skew span improved the pressure fluctuation characteristics. Nevertheless, given the relatively optimized nature of the original design, the improvements achieved by the optimized designs were marginal. Specifically, the maximum speed increased by approximately 1%, and the amplitude of the pressure fluctuations decreased by about 9%.

Table 11. Comparison of design parameters and performance for the selected optimization schemes.

Scheme		Design Parameters				Performance Results		
		Diameter (m)	Effective Pitch	Area Ratio	Skew Span (°)	Maximum Speed (kn)	Rotation Speed (r/min)	Fluctuating Pressure at 1BPF (kPa)
Original propeller		10.80	0.7894	0.386	24.91	14.78	57.49	2.24
Optimization schemes	Opt1	11.02	0.7616	0.438	29.42	14.91	56.51	2.03
	Opt2	12.00	0.6998	0.300	28.59	15.75	57.5	3.26
	Opt3	9.50	1.0042	0.500	30.00	13.98	57.86	1.68

7. Conclusions

The existing machine learning-based propeller hydrodynamic performance prediction models still require further enhancement due to issues such as data quality limitations and insufficient physical constraints. This study employed a high-quality, fully physical open-water performance test dataset which was augmented with publicly available propeller data. For the prediction of a propeller's open-water thrust and torque coefficients, both single-task and multitask prediction models based on ANNs were developed. A comparison of the two models in terms of prediction accuracy and physical reliability was performed. Additionally, the generalization capability of the multitask model in predicting open-water performance for unknown propellers was analyzed. On this basis, a multitask model was utilized to establish a multi-objective optimization design process for propellers. An optimization design application was conducted for a 325,000 ton VLOC's propeller. The key conclusions drawn from this study are as follows:

(1) The use of propeller charts significantly enhances and expands the parameter space of the dataset. By applying a quadratic polynomial with the advance coefficient as the variable, high-precision fitting of the propeller thrust coefficient and torque coefficient curves was achieved, with a fitting truncation error of approximately 4%. As a result, the

coefficients of the quadratic polynomial can be utilized as prediction targets in the rapid prediction model.

(2) An analysis of the prediction capabilities of the multitask and single-task models revealed that the multitask model outperformed the single-task model. The average prediction error for the thrust coefficient decreased from 2.61 to 2.07, that for the torque coefficient decreased from 3.58 to 2.31, and that for the efficiency decreased from 3.04 to 2. Additionally, the peak errors were also reduced. Moreover, the predicted curvature of the performance curves obtained from the multitask model closely matched the experimental results, effectively eliminating the abnormal fluctuations observed in the single-task mode.

(3) For the three unknown propeller designs outside of the training dataset, the prediction results of the multitask model aligned well with the experimental results. The predicted deviation for the thrust coefficient was within 2.2%, that for the torque coefficient was within 4.6%, and that for the efficiency was within 3.8%, effectively validating the model's generalization capability.

(4) The multitask model was applied to propeller optimization design for ships, successfully generating a Pareto front solution set for the maximum ship speed and induced fluctuating pressure. This demonstrates the application potential of the multitask model in propeller optimization design.

It is worth noting that the current multitask model still exhibited relatively high prediction errors for certain propeller designs and overly smoothed performance curve fluctuations. In the future, efforts will focus on continuously enhancing the training dataset, refining the geometric feature input parameters, and increasing the polynomial fitting order for the open-water performance curves. These improvements are expected to further enhance the predictive accuracy of the multitask learning network model.

Author Contributions: Conceptualization, C.W. and Y.C.; methodology, L.L.; software, L.L.; validation, L.H. and Q.H.; formal analysis, L.H.; investigation, Q.H.; resources, Y.C.; data curation, L.H.; writing—original draft preparation, L.L.; writing—review and editing, C.W. and D.T.; visualization, L.L.; supervision, C.W.; project administration, Y.C.; funding acquisition, Y.C. All authors have read and agreed to the published version of the manuscript.

Funding: This research received no external funding.

Institutional Review Board Statement: Not applicable.

Informed Consent Statement: Not applicable.

Data Availability Statement: Code for data analysis is available on request from the authors.

Conflicts of Interest: The authors declare no conflicts of interest.

Nomenclature

A_E	Area of stretched profile for propeller blade
A_o	Propeller disc area
C	Chord length of propeller section
$C_{T1} \sim C_{T3}$	Coefficients of quadratic polynomial for thrust coefficient
$C_{Q1} \sim C_{Q3}$	Coefficients of quadratic polynomial for 10 fold torque coefficient
D	Propeller diameter
f_{max}	Maximum camber of propeller section
f_E	Effective camber
H_r	Hub ratio of propeller
J	Advance coefficient
k	Curve curvature
K_T	Thrust coefficient

K_Q	Torque coefficient
lr_0	Initial learning rate
lr	Learning rate
$MAPE$	Mean Absolute Percentage Error
MSE	Mean Squared Error
P	Pich of propeller section
P_E	Effective pitch
R	Propeller radius
t	Current iteration number
T	Total number of iterations
T_{max}	Maximum thickness of propeller section
y'	First derivative
y''	Second derivative
$\hat{y}_i$	Predicted value or fitted value
y_i	True value
Z_R	Local rake of propeller section
Z_{Ta}	Rake span
Z_T	Total rake of propeller section
η	Efficiency
θ_s	Skew angle
θ_{sa}	Skew span
β_p	Pitch angle of propeller section
σ	Standard deviation
μ	Mean of the input variable
α	Innovation parameter

References

1. Molland, A.F.; Turnock, S.R.; Hudson, D.A. *Ship Resistance and Propulsion*; Cambridge University Press: Cambridge, UK, 2017.
2. Papanikolaou, A. *Ship Design: Methodologies of Preliminary Design*; Springer: Berlin/Heidelberg, Germany, 2014.
3. Lee, S.S. Analysis of the effects of EEDI and EEXI implementation on CO_2 emissions reduction in ships. *Ocean Eng.* **2024**, *295*, 116877. [CrossRef]
4. Barnitsas, M.M.; Ray, D.; Kinley, P. *KT, KQ and Efficiency Curves for the Wageningen B-Series Propellers*; University of Michigan: Ann Arbor, MI, USA, 1981.
5. Kinnas, S.A. A general theory for the coupling between thickness and loading for wings and propellers. *J. Ship Res.* **1992**, *36*, 59–68. [CrossRef]
6. Dang, J.; Brouwer, J.; Bosman, R.; Pouw, C. Quasi-steady two-quadrant open water tests for the Wageningen Propeller C-and D-series. In Proceedings of the Twenty-Ninth Symposium on Naval Hydrodynamics, Gothenburg, Sweden, 26–31 August 2012.
7. Stajuda, M.; Karczewski, M.; Obidowski, D.; Jóźwik, K. Development of a CFD model for propeller simulation. *Mech. Mech. Eng.* **2016**, *20*, 579–593.
8. Li, L.; Zhou, B.; Liu, D.; Wang, C. Numerical Analysis of Influence of the Hull Couple Motion on the Propeller Exciting Force Characteristics. *J. Mar. Sci. Eng.* **2019**, *7*, 330. [CrossRef]
9. Shen, Z.; Wan, D.; Carrica, P.M. Dynamic overset grids in OpenFOAM with application to KCS self-propulsion and maneuvering. *Ocean Eng.* **2015**, *108*, 287–306. [CrossRef]
10. Yang, R.Y.; Shen, H.C.; Yao, H.Z. Uncertain analysis of CFD simulation on the open-water performance of the propeller. *J. Ship Mech.* **2010**, *14*, 472–480.
11. Zhang, Z.; Hong, F.; Tang, D. *PreFluP–Preprocessing Program for the RANSE Simulation of Marine Propulsors. Report and User's Guide'*; CSSRC: Denver, CO, USA, 2007.
12. Tu, T.N.; Chien, M.N.M. *EEDI Reduction by Investigating the Capability of RANSE CFD for Propeller, Propeller–Hull Form Performance Calculation During Ship Optimization Process*; IAMU: Tokyo, Japan, 2017; p. 253. Available online: https://scholarworks.calstate.edu/downloads/sq87bv679#page=259 (accessed on 7 January 2025).
13. Guan, G.; Zhang, X.; Wang, P.; Yang, Q. Multi-objective optimization design method of marine propeller based on fluid-structure interaction. *Ocean Eng.* **2022**, *252*, 111222. [CrossRef]
14. Gurgen, S.; Altin, I.; Ozkok, M. Prediction of main particulars of a chemical tanker at preliminary ship design using artificial neural network. *Ships Offshore Struct.* **2018**, *13*, 459–465. [CrossRef]

15. Parkes, A.I.; Sobey, A.J.; Hudson, D.A. Physics-based shaft power prediction for large merchant ships using neural networks. *Ocean Eng.* **2018**, *166*, 92–104. [CrossRef]
16. Rawson, A.; Brito, M.; Sabeur, Z.; Tran-Thanh, L. A machine learning approach for monitoring ship safety in extreme weather events. *Saf. Sci.* **2021**, *141*, 105336. [CrossRef]
17. Feng, F.; Huang, S.; Hu, J. Application of artificial neural network to design of Propeller. *J. Harbin Eng. Univ.* **2002**, *23*, 1–4.
18. Koushan, K. Mathematical expressions of thrust and torque of Newton-Rader propeller series for high speed crafts using artificial neural networks. In Proceedings of the 8th International Conference on Fast Sea Transportation (FAST 2005), St. Petersburg, Russia, 27–30 June 2005.
19. Koushan, K. Mathematical expressions of thrust and torque of Gawn-Burrill propeller series for high speed crafts using artificial neural networks. In Proceedings of the 9th International Conference on Fast Sea Transportation (FAST 2007), Shanghai, China, 23–27 September 2007.
20. Roddy, R.F.; Hess, D.E.; Faller, W. Neural network predictions of the 4-quadrant Wageningen propeller series. *Naval Surface Warfare Center Carderock Division, Hydromechanics Department Report NSWCCD-50-TR-2006/004*. 2006. Available online: https://apps.dtic.mil/sti/pdfs/ADA455497.pdf (accessed on 7 January 2025).
21. Zeng, Z.B.; Ding, E.B.; Tang, D.H. Ship propeller design optimization based on BP neural network and genetic algorithm. *J. Ship Mech.* **2010**, *14*, 20–27.
22. Valčić, M.; Dejhalla, R. Neural network prediction of open water characteristics of ducted propeller. *Pomor. Zb.* **2015**, *49*, 101–115. [CrossRef]
23. Li, L.; Chen, Y.; Qiang, Y.; Zhou, B.; Chen, W. Construction and application of numerical diagram for high-skew propeller based on machine learning. *Ocean Eng.* **2023**, *278*, 114480. [CrossRef]
24. Bakhtiari, M.; Ghassemi, H. CFD data based neural network functions for predicting hydrodynamic performance of a low-pitch marine cycloidal propeller. *Appl. Ocean Res.* **2020**, *94*, 101981. [CrossRef]
25. Qiang, Y.; Chen, S.; Chen, Y.; Chu, X. Prediction of open-water characteristics of ship propellers based on machine learning surrogate model. *Shipbuild. China* **2022**, *63*, 181–188.
26. Qiang, Y.; Xie, S.; Li, L.; Xia, H.; Chen, Y. Application of dimension reduction methods on propeller performance prediction model. *Ocean Eng.* **2024**, *291*, 116310. [CrossRef]
27. Li, L.; Chen, Y.; Xie, S.; Xiao, Y.; Fang, T.; Wang, C. Comprehensive feature-based machine learning for fast prediction of marine propeller's open-water performance. *Appl. Ocean Res.* **2025**, *154*, 104310. [CrossRef]
28. Caruana, R. Multitask learning: A knowledge-based source of inductive bias1. In Proceedings of the Tenth International Conference on Machine Learning, Amherst, MA, USA, 27–29 July 1993; pp. 41–48.
29. Caruana, R. Multitask learning. *Mach. Learn.* **1997**, *28*, 41–75. [CrossRef]
30. Nunes, M.; Gerding, E.; McGroarty, F.; Niranjan, M. A comparison of multitask and single task learning with artificial neural networks for yield curve forecasting. *Expert Syst. Appl.* **2019**, *119*, 362–375. [CrossRef]
31. Ilias, L.; Askounis, D. Explainable identification of dementia from transcripts using transformer networks. *IEEE J. Biomed. Health Inform.* **2022**, *26*, 4153–4164. [CrossRef] [PubMed]
32. Paredes B R, Argyriou A, Berthouze N; Pontil M. Exploiting unrelated tasks in multi-task learning//Artificial intelligence and statistics. *PMLR* **2012**, *22*, 951–959.
33. Miglianti, L.; Cipollini, F.; Oneto, L.; Tani, G.; Gaggero, S.; Coraddu, A.; Viviani, M. Predicting the cavitating marine propeller noise at design stage: A deep learning based approach. *Ocean Eng.* **2020**, *209*, 107481. [CrossRef]
34. Ilias, L.; Kapsalis, P.; Mouzakitis, S.; Askounis, D. A Multitask Learning Framework for Predicting Ship Fuel Oil Consumption. *IEEE Access* **2023**, *11*, 132576–132589. [CrossRef]
35. Liu, T.; Xu, X.; Lei, Z.; Zhang, X.; Sha, M.; Wang, F. A multi-task deep learning model integrating ship trajectory and collision risk prediction. *Ocean Eng.* **2023**, *287*, 115870. [CrossRef]
36. Shen, Y.D.; Zhou, L.D. On the method of the mathematical presentation for propeller design diagrams. *Shipbuild. China* **1994**, *51*, 68–75.
37. Vesting, F.; Gustafsson, R.; Bensow, R.E. Development and application of optimisation algorithms for propeller design. *Ship Technol. Res.* **2016**, *63*, 50–69. [CrossRef]
38. Mello, R.F.; Ponti, M.A. *Machine Learning: A Practical Approach on the Statistical Learning Theory*; Springer: Berlin/Heidelberg, Germany, 2018.
39. Bassam, A.M.; Phillips, A.B.; Turnock, S.R.; Wilson, P.A. Artificial neural network based prediction of ship speed under operating conditions for operational optimization. *Ocean Eng.* **2023**, *278*, 114613. [CrossRef]
40. Cepowski, T. The prediction of ship added resistance at the preliminary design stage by the use of an artificial neural network. *Ocean Eng.* **2020**, *195*, 106657. [CrossRef]
41. Eckle, K.; Schmidt-Hieber, J. A comparison of deep networks with ReLU activation function and linear spline-type methods. *Neural Netw.* **2019**, *110*, 232–242. [CrossRef] [PubMed]

42. Jais IK, M.; Ismail, A.R.; Nisa, S.Q. Adam optimization algorithm for wide and deep neural network. *Knowl. Eng. Data Sci.* **2019**, *2*, 41–46. [CrossRef]
43. Zhou, Z.; Zhang, W.; Yao, P.; Long, Z.; Bai, M.; Liu, J.; Yu, D. More realistic degradation trend prediction for gas turbine based on factor analysis and multiple penalty mechanism loss function. *Reliab. Eng. Syst. Saf.* **2024**, *247*, 110097. [CrossRef]
44. Alvarellos, A.; Figuero, A.; Sande, J.; Peña, E.; Rabuñal, J. Deep learning based ship movement prediction system architecture. In *International Work-Conference on Artificial Neural Networks*; Springer International Publishing: Cham, Swtizerland, 2019; pp. 844–855.
45. Yang, J.; Wang, F. Auto-ensemble: An adaptive learning rate scheduling based deep learning model ensembling. *IEEE Access* **2020**, *8*, 217499–217509. [CrossRef]
46. Chen, C.; He, C.; Hu, C.; Pei, H.; Jiao, L. A deep neural network based on an attention mechanism for SAR ship detection in multiscale and complex scenarios. *IEEE Access* **2019**, *7*, 104848–104863. [CrossRef]
47. Dalheim, Ø.; Steen, S. Preparation of in-service measurement data for ship operation and performance analysis. *Ocean Eng.* **2020**, *212*, 107730. [CrossRef]
48. Xue, Q.; Gu, X.; Zhou, B.; Wu, S. Empirical prediction of propeller induced pressure fluctuation based on non-linear regression analysis. In Proceedings of the Thirty-One TH National Symposium on Hydrodynamics (Part II), Val de Reuil, France, 17–22 September 2000; pp. 364–373.